Sánchez-Prieto, J., Soria-Verdugo, A., Briongos, J. V., & Santana, D. (2015). Stagnant regions estimation in fluidized beds from bed surface observation. *Chemical Engineering Journal*, 281, 109-118.

DOI: 10.1016/j.cej.2015.06.097

Stagnant regions estimation in fluidized beds from bed surface observation

J. Sánchez-Prieto, A. Soria-Verdugo, J.V. Briongos, D. Santana

Universidad Carlos III de Madrid, Thermal and Fluid Engineering Department, Avda. de la Universidad 30, 28911 Leganés (Madrid), Spain

Abstract

A novel approach to estimate the size of stagnant regions in large-scale fluidized beds by means of exper-imental data obtained from images recorded on the bed surface was presented. For this purpose, the internal structure of an induced maldistributed pseudo-2D fluidized bed was first studied. Half of the total distributor area was covered to generate an induced stagnant region. The size and shape of this area was studied for several relative gas velocities and bed aspect ratios. The defluidized area was found to be almost independent of the bed aspect ratio, however, it was found to decrease for higher relative gas velocities. A solids recirculation zone was also found above the defluidized zone. The size of this zone increases with relative gas velocity, suggesting that it is strongly related to bubble motion. A correlation was developed to relate the visible bubble flow to the size of the defluidized zone. The results obtained in the 2D bed were extrapolated to a 3D cylindrical fluidized bed with a half-covered distributor plate to estimate the volume of the defluidized zone. The visible bubble flow in the 3D facility was estimated. Using the proposed correlation for the defluidized volume in the 2D bed was used to estimate the deflu-idized volume in the 3D bed. Finally, the calculated values of the defluidized volume were compared with the experimental values in the 3D facility, obtaining a maximum relative error of 20% in the estimations.

Keywords: Fluidization, Maldistribution, Digital image analysis, PIV

Graphical abstract

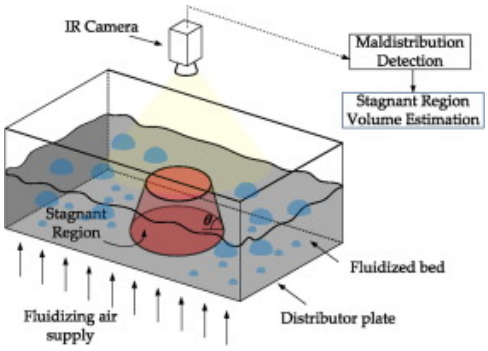

*Corresponding author. Tel: +34 916246032.
Email address: jsprieto@ing.uc3m.es (J. Sánchez-Prieto).

Notation

A_t	distributor cross-sectional area [m^2]
a_i	area of the ith bubble cut by the horizontal section de-fined [m^2]
	bubble concentration [–]
$\overline{B}$	black beads concentration [–]
C	penetration ratio [–]
d	bed diameter [m]
D	bubble diameter [m]
D_b	mean particle diameter [l̇m]
d_P	parameter of the Johnsson's et al. correlation [–] height over the
f_2	distributor plate [m]
h	height of the 2D bed [m]
H	fixed bed height [m]
H_0	aspect ratio 3D [–]
H_0/D	aspect ratio 2D [–]
H_0/W	number of images in each video [–]
N	number of orifices of the distributor plate [–] distributor pressure
N_h	drop [kPa]
DP_{dist}	visible bubble flow [m^3/s]
Q_b	bed radius [m]
r	pressure drop ratio [–]
R	air superficial velocity [m/s]
U_0	rising bubble velocity [m/s]
U_b	superficial gas velocity at which all the distributor orifices became
U_M	operative [m/s]
	minimum fluidization velocity [m/s]
U_{mf}	relative fluidization velocity [–]
U_r	
U_{vis}	visible bubble flow [m/s]
|V|	time-averaged dense phase velocity [m/s]
V_{def}	volume of the defluidized zone [m^3]
V_{rec}	volume of the recirculation zone [m^3]
V_t	total solids volume [m^3]
W	width of the 2D bed [m]
x	distance between the bed wall and the boundary of black
	beads [m]
x_f	distance between the centre of the bed and the bound-ary of
	defluidized zone [m]
Z	thickness of the 2D bed [m]

Greek letters

w	fraction of visible bubble flow [–] black
q_{bb}	beads density [kg/m^3] particle density
q_s	[kg/m^3] penetration angle [°]
h	

Abbreviations

BFB	bubbling fluidized bed digital
DIA	image analysis full-scale span
FSS	infrared
IR	particle image velocimetry
PIV	

1. Introduction

Gas maldistribution is one of the most common problems related to distributor design and has an important effect on the performance of fluidized beds. Maldistribution is industrially undesirable: for dryers, because in the dead zones the drying rate drastically decreases, for reactors, because bypassing of reactants and uneven temperature in the bed are obtained, and in general, because it affects the heat and mass transfer capabilities and it may lead to defluidization and agglomeration problems. In most of the industrial processes carried out in fluidized beds, it is of crucial importance to prevent defluidization. When a defluidization problem is not detected and solved, major damage can be caused to bed internals, agglomeration of bed particles may occur and, as a consequence, the heat and mass transfer capabilities of the bed will be drastically reduced [1].

Maldistribution of gas and the design criteria to avoid it have been investigated by many researchers, such as [2], [3], [4], [5]. Thorpe et al. [5] reviewed the existing literature concerning theoretical models used to estimate the boundary of maldistribution in fluidized beds. The authors determined UM, defined as the superficial velocity at which all the orifices or tuyeres of the distributor plate become operative, which usually means they are jetting [6], [7], with bed pressure drop measurements in a 3D fluidized bed and compared the experimental results with predictions of several models: the theory of Fakhimi and Harrison [3], the theory of Whitehead and Dent [2] and the theory of Yue and Kolaczwoski [4]. They found the best fit with the theory of Fakhimi and Harrison. They also found a good agreement with the theory of Yue and Kolaczwoski, however, this theory is an attempt to improve the theory of Fakhimi and Harrison by considering the effect of bed height. The authors concluded that the theory of Fakhimi and Harrison gives the best estimation, since it is a simpler theory than that of Yue and Kolaczwoski. These works were based on the study of UM, which depends on the gas flow rate, the bed aspect ratio, the bed material and the open area of the distributor. All these variables have been studied in terms of the distributor to bed pressure drop ratio, R, since the onset of maldistribution seems to be directly related to this ratio [8].

A recent work of Sánchez-Prieto et al. [9] showed that gas maldistribution in fluidized beds can be detected using pressure signal analysis. The authors studied the onset of maldistribution with digital image analysis (DIA) of images of the bed surface and then, applied several monitoring methods to quantify the boundary between stable operation and maldistribution. However, nothing can be said about the internal structure of the maldistribution region generated inside the bed, since the pressure fluctuations signals were proven to detect if there is maldistribution present but could not identify the exact source of these changes in the dynamical behavior.

Visualization methods such infrared (IR) imaging are commonly used in industrial boilers and incinerators for monitoring and control purposes [10]. These methods are usually employed to obtain information about the combustion flame [11], [12], [13], [14], since it is directly related to the combustion performance. IR imaging can also be used to determine temperature profiles of solid bodies such as the solid fuel particles, the reactor wall or, in case of a fluidized bed combustor, the bed material. Thus, the online monitoring of the bed surface of a fluidized bed combustor with an IR camera can help to detect dead zones caused by gas maldistribution or agglomeration.

In this work a new methodology is proposed to study the defluidized zone generated in an induced maldistributed pseudo-2D fluidized bed. These beds have shown to be of great importance for the understanding of fluidized beds. Two-dimensional beds typically have a transparent wall and possess a small thickness, so that optical access to the system is allowed and the behavior of the visualized particles is representative of the whole system [15]. The variables affecting the defluidized zone in a pseudo-2D fluidized bed were investigated to obtain a correlation for the size of this zone. The final aim of this work is the extrapolation of the 2D results to a 3D fluidized bed, in order to obtain a method capable of estimating the size of the defluidized zone in an industrial fluidized bed combustor, provided that experimental images of the bed surface are available.

2. Experimental setup

Two different experimental facilities were employed in this work: a pseudo-2D cold fluidized bed and a lab-scale cylindrical bubbling fluidized bed (BFB).

The dimensions of the pseudo-2D cold fluidized bed were 0.3 m × 1 m × 0.01 m (width W, height H, and thickness Z). The bed material employed was ballotini glass particles of 2500 kg/m3 density and a mean diameter of 700 μm (600–800 μm), classified as type B according to Geldart's classification [16]. The air flow was measured with a set of two flow meters, with ranges of 0–200 L/min and 0–500 L/min providing an accuracy of 1% of full-scale span (FSS). The air distributor consists of a perforated plate with two rows of 30 holes of 0.001 m in diameter, arranged in a triangular configuration with 0.01 m pitch. The variation of the pressure drop with gas superficial velocity was determined with pressure measurements ($\Delta P_{dist} = 4.65 U_0^2$). The distributor is equipped with a mesh to avoid the falling of particles inside the plenum chamber and to ensure a proper distributor to bed pressure drop ratio, R, to avoid gas maldistribution [8], [17]. The front and rear walls of the bed were made of glass and the rear wall was painted in black to increase the contrast of the images recorded at the front. A Basler A640 digital camera was used to record images of the front wall of the fluidized bed at 100 fps. The spatial resolution of the pictures is 360 × 640 pixels. A uniform illumination of the front of the bed was guaranteed with the use of two spotlights of 650 W.

The plenum chamber was divided in two separated chambers of the same size to produce an induced maldistribution similar to that studied in Sánchez-Prieto et al. [9], where half of the total number of orifices of the distributor plate was covered. In the experiments performed in this work, the air was only supplied to the left chamber (half of the total distributor area and orifices) and, therefore, bubbles were generated only at the left side of the bed. The right chamber, where no air was supplied, induces a defluidized zone at the right side of the bed. A schematic diagram of the pseudo-2D bed is shown in Fig. 1(a).

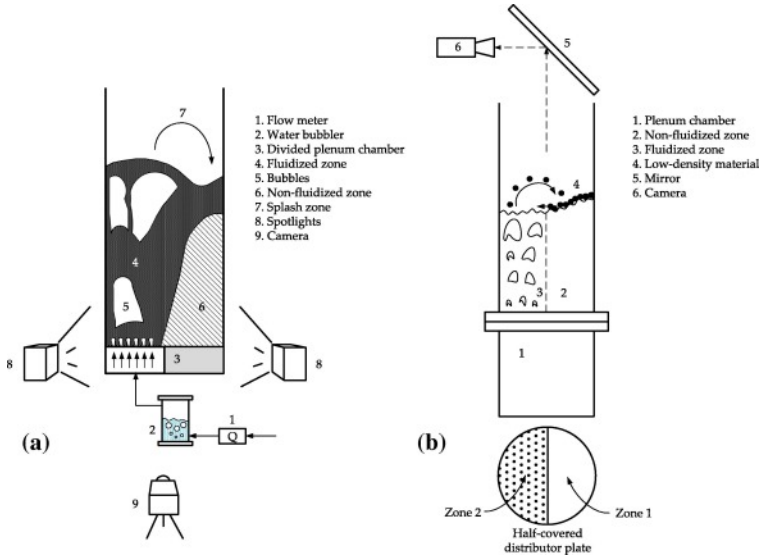

Fig. 1. Schematic diagram of the experimental setup: 2D facility (a) and 3D facility (b).

In each experiment, the bed was filled with ballotini glass beads at the desired bed aspect ratio. The fluidizing air enters the bed across the left side of the plenum chamber with a fixed flow rate. When the bed is operating at the steady state, a handful of black painted ballotini particles were introduced from the top of the bed. These black particles have the same mean diameter, density and size as the rest of the particles used in the experiment, being the color the only difference between them. The black painted particles mix with the dense phase just in the zones where motion of particles occurs. As a result, the defluidized zone remains white whereas the rest of the particles become a mixture of black and white (Fig. 2), obtaining a contrast between the defluidized zone and the rest of the bed. This methodology facilitates the recognition of the defluidized zone in the thresholded images.

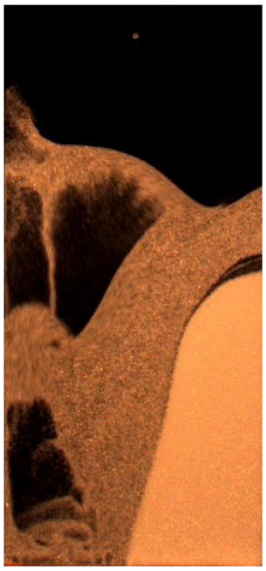

Fig. 2. Example of an image after adding the black painted particles.

Experiments were also carried out in a lab-scale cylindrical bubbling fluidized bed (BFB), with a bed diameter of 0.192 m, previously described in Sánchez-Prieto et al. [9]. The variation of the pressure drop with gas superficial velocity was determined with pressure measurements ($\Delta P_{dist} = 2.17U^0_2$). A schematic of the 3D facility is shown in Fig. 1(b). The bed material used was sepiolite (clay) particles (SG36) with a density of 1551 kg/m3 and 450 μm mean diameter, classified as type B according to Geldart's classification [16].

The main physical properties of the bed material used in both experimental facilities are summarized in Table 1, including experimental values of the minimum fluidization velocity, Umf, at ambient temperature. The minimum fluidization velocity of ballotini particles was measured in the 2D facility while the minimum fluidization velocity of the sepiolite particles was measured in the lab-scale cylindrical BFB. The orifices of half the cross sectional area were covered in both experimental facilities to create an induced maldistributed region.

Table 1. Physical properties of solid particles.

	dp [μm]	**ρs [kg/m3]**	**Geldart type**	**Umf [m/s]**
Ballotini glass beads	700	2500	B	0.44
Sepiolite (SG36)	450	1551	B	0.13

Black beads of 0.006 m in diameter made of a low-density material (ρbb = 36.20 kg/m3, ε0 = 0.35) were used to produce a high contrast in the bed surface, which facilitate the recognition of erupting bubbles during the digital analysis of the images recorded. When a bubble explodes at the bed surface, the black beads are ejected leaving a free space proportional to the size of the exploding bubble. The bed surface was recorded to obtain an average solid concentration profile used to estimate the boundary between the fluidized and non-fluidized zones [9].

Table 2. Summary of the experimental conditions.

Facility	Aspect ratio (H0/W; H0/D)	Relative velocity (Ur)	Bed material
Pseudo-2D bed	0.50; 0.75; 1.00; 1.25	3.00; 4.00; 5.00; 6.00	Ballotini glass beads
Cylindrical BFB	0.50; 0.75; 1.00; 1.25	2.50; 3.00; 3.50; 4.00	Sepiolite (SG36)

3. Results and discussion

3.1. Defluidized and recirculation zones in pseudo-2D beds

The images recorded in the 2D facility (see Supplementary Material) were binarized, summed and rescaled with the total number of images processed, producing a time-averaged image that represents the fraction of time that a point of the bed is occupied by dense phase, $C(x,y) = \sum_{i=1}^{N} C_i(x,y)/N$, where N is the number of images. Therefore, the fraction of time that a point is occupied by bubbles is defined by B = 1 - C . B and C will be, respectively, the bubble and dense phase concentration [15]. A similar analysis was performed for the images of the bed surface recorded in the cylindrical BFB.

The dense phase concentration profiles, C, are shown in Fig. 3(a) for the case of H0/W=0.75 (the nominal case hereafter). As can be seen, as long as the relative gas velocity, Ur, is increased the high bubble concentration region (cold colour) increases. It is worth to notice that bubbles only appear in the left side of the bed, where the air is supplied. The right side, where a higher solid concentration is achieved, corresponds to the defluidized zone generated as a consequence of the blocked part of the plenum chamber.

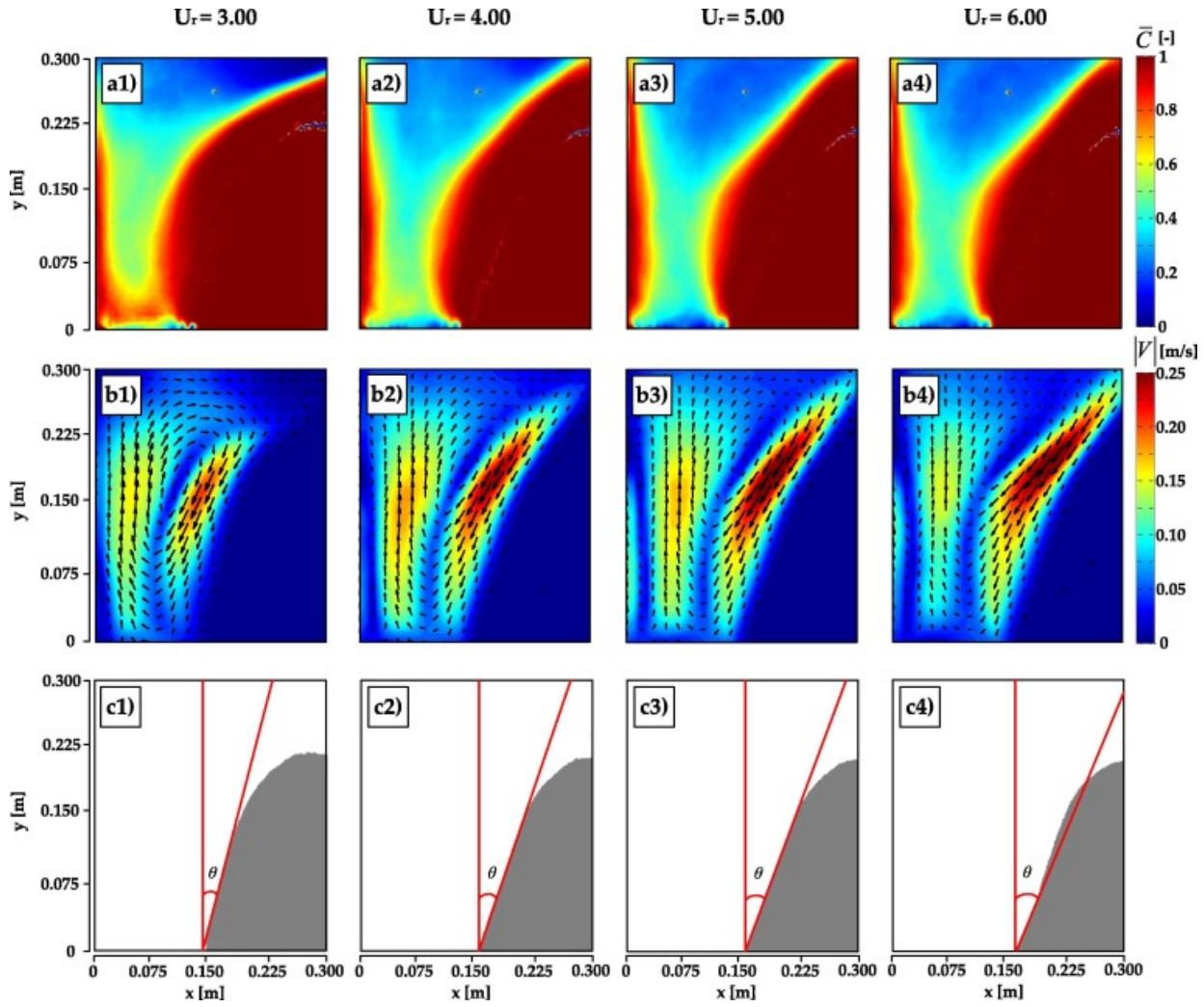

Fig. 3. Dense phase concentration profiles (a), time-averaged dense phase velocity profiles (b) and defluidization area and penetration angle (c) for the different relative gas velocities tested (H0/W = 0.75).

The dense phase velocity profiles were also obtained by means of the multigrid PIV code MATPIV [18]. Interrogation windows of 16 × 16 pixels with a 50% overlap were used in the PIV analysis. In Fig. 3(b) the time-averaged dense phase velocity contours are presented together with the time-averaged dense phase velocity vectors. The time-averaged dense phase velocity was calculated averaging the instantaneous velocities obtained by PIV, as described in Laverman et al. [19]. As can be seen, there is a vortex of solids in all cases, indicating the presence of a solids recirculation zone just above the defluidized zone. The defluidized zone can also be detected in the dense phase velocity profiles as a dark blue zone, where the time-averaged dense phase velocity is zero. Both the dense phase velocity in the recirculation zone and the size of this zone increases for higher relative gas velocities due to the more vigorous fluidization imposed by bigger bubbles [20]. As long as the solids movement in a fluidized bed is induced by the bubbles, it seems that the size of the recirculation zone is strongly related to the bubble size. These zones were previously identified in tapered fluidized beds [21], [22], [23].

A proper threshold was applied to the images to distinguish the defluidization zone. Taking into account that black painted particles are only present in the zone where the dense phase is moving, the defluidized zone is completely white (Fig. 2). The results for the defluidized zone of the nominal case and for all the relative gas velocities tested are shown in Fig. 3(c). As can be observed, the defluidized area decreases as long as the relative gas velocity increases because of the higher capability of greater bubbles to move dense phase. The height of the defluidization zone remains almost constant with the relative gas velocity, but the angle with the normal to the distributor increases with relative gas velocity. Additionally, the penetration angle, θ, has been plotted in Fig. 3(c). This penetration angle is defined as the angle between the boundary of the defluidized zone and the normal to the distributor of the bed. The penetration angle is proportional to the relative gas velocity and, therefore, inversely proportional to the defluidized area.

The penetration angle measured in the pseudo-2D bed (Fig. 3(c)) as a function of the dimensionless excess gas velocity is shown in Fig. 4 for all the bed aspect ratios tested. It was found that the variation of the penetration angle with the relative gas velocity is almost independent of the bed aspect ratio. Therefore, a correlation is proposed to estimate the penetration angle as a function of the dimensionless excess gas velocity (Eq. (1)), considering the theoretical assumption that the penetration angle should be zero when the bed is operated at minimum fluidization conditions.

$$\theta[\mathrm{deg}] = 5.5(Ur - 1) \tag{1}$$

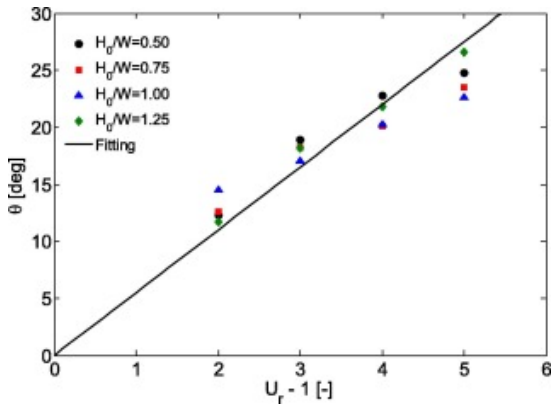

Fig. 4. Penetration angle as a function of the different relative gas velocities tested. Solid lines correspond to the correlation proposed.

It should be noticed that the proposed linear correlation is only valid in the range of gas superficial velocities investigated (Ur = 3–6).

The defluidized area was estimated from the time-averaged thresholded images shown in Fig. 3(c). These values were multiplied by the bed thickness to obtain the defluidized volume and then normalized with the average volume occupied by dense phase (i.e. the average volume of the expanded bed). The normalized defluidized volume obtained is plotted in Fig. 5(a) as a function of the relative gas velocity for the different aspect ratios investigated. As can be seen, the defluidized volume decreases with the relative gas velocity, following a similar trend for all the aspect ratios. For aspect ratios of 0.75, 1.00 and 1.25 the results of the defluidized volume are very similar, however, for an aspect ratio of 0.50 the results show a slight deviation which might be attributed to a different bubble coalescence in this case, as stated by Pallarès and Johnsson [24] who found that several bubble paths appeared in shallow beds.

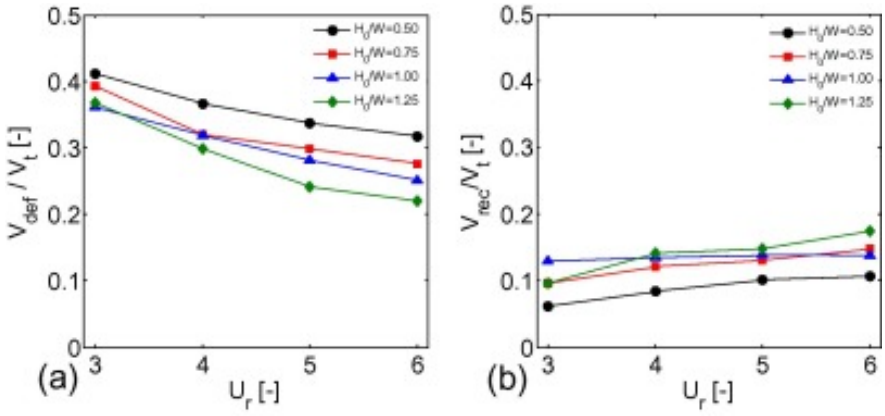

Fig. 5. Normalized defluidized volume (a) and normalized recirculation volume (b) as a function of relative gas velocity for the different aspect ratios tested.

The recirculation area was defined as the high downwards velocity area located over the defluidized area (Fig. 3(b)) and it was estimated applying a threshold (i.e. half of the maximum dense phase velocity in each case) to the time-averaged dense phase velocity contours. The results were also multiplied by the bed thickness to obtain the recirculation volume and normalized with the average expanded bed volume. The normalized recirculation volume as a function of the relative gas velocity for the aspect ratios investigated is shown in Fig. 5(b). The recirculation volume increases with the relative gas velocity, as a result of an increase in bubble size and, consequently, in solids motion. As for the defluidized volume, the results for aspect ratios of 0.75, 1.00 and 1.25 were very similar, whereas differences were observed for the case of aspect ratio of 0.50. These results suggest that both defluidized and recirculation volumes are independent of the bed aspect ratio provided that the bed aspect ratio is high enough to guarantee that a single bubble path is formed due to bubble coalescence.

In order to relate the bubble parameters with the aforementioned regions, the visible bubble flow, Qb, was calculated in the 2D bed using Eq. (2), as described in Sánchez-Delgado et al. [25].

$$Q_b = \frac{1}{N}\sum_{j=1}^{N}\sum_{i=1}^{n} U_{bi} a_i \qquad (2)$$

where a_i is the area of the ith bubble cut by the horizontal section defined (i.e. at H_0), U_{bi} is the vertical bubble velocity, N is the number of images and n is the number of bubbles passing through the horizontal section at jth image. The area of the ith bubble cut by the horizontal section was estimated with the measured values of the bubble diameter D_b as the product of the generated arc between the bubble and the horizontal section and the bed thickness. The average bubble diameter, D_b, was obtained by means of DIA of the images recorded at the front wall of the bed and the average bubble velocity, U_b, was calculated using bubble tracking. The visible bubble flow in velocity units, U_{vis}, can be obtained dividing Q_b by the bed cross section, in this case the cross section of the active zone of the distributor plate (i.e. half of the total cross-sectional area of the bed). The throughflow, U_{th}, was then estimated as a function of the visible bubble flow, the gas superficial velocity and the minimum fluidization velocity with Eq. (3).

$$U_{th} = U_0 - U_{mf} - U_{vis} \tag{3}$$

The experimental values of U_{th} were normalized with the minimum fluidization velocity and plotted as a function of the relative gas velocity, $U_{r,}$ in Fig. 6. The correlation proposed by Sánchez-Delgado et al. [25], which can be applied to beds operating at a bubbling regime, was also plotted in Fig. 6 for comparison. The experimental results of the throughflow seem to be in agreement with the predicted values of the correlation. The differences found might be attributed to the fact that the correlation of Sánchez-Delgado et al. [25] was developed for values of the visible bubble flow calculated at a height of $(2/3)H_0$. In view of the results showed in Fig. 6, the variation of the throughflow with the bed aspect ratio can be neglected in pseudo-2D beds.

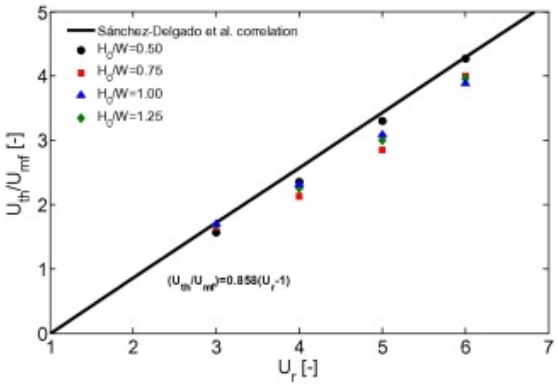

Fig. 7. Normalized defluidized volume as a function of the normalized visible bubble flow for all the aspect ratios tested.

The normalized defluidized volume seems to follow a linear trend with the normalized visible bubble flow in the range of operation investigated. Taking into account that the relative gas velocities used in the 3D facility are similar to those used to develop the correlation, the linear fit is expected to give good predictions for the 3D facility. To extrapolate these results to a 3D bed, a relation between the normalized defluidized volume and the normalized visible bubble flow was obtained (Eq. (4)).

$$\left(\frac{V_{def}}{V_t}\right) = -0.11\left(\frac{U_{vis}}{U_{mf}}\right) + 0.41 \tag{4}$$

3.2. Extrapolation to 3D bed data

The final aim is to develop a method capable of predicting the size of dead zones, caused by gas maldistribution or agglomeration, in large-scale fluidized beds using visual information of the bed surface. First, the validity of extrapolating the results of the defluidized volume obtained in the pseudo-2D bed to a lab-scale cylindrical bubbling fluidized bed (BFB) was evaluated. The extrapolation was made through a comparison of two variables: the penetration angle and the defluidized volume.

The experiments described in the experimental setup section for the 3D bed were carried out in this section. For each aspect ratio and relative gas velocity, the time-averaged black beads concentration was obtained in the bed surface by means of DIA, as shown in Fig. 8(a). The penetration ratio, d, is defined as the distance between the bed wall and the boundary of black beads, x, divided by the bed diameter, D (Fig. 8(b)). The penetration ratio was used to estimate the penetration angle, defined previously for the 2D bed. In the 2D bed the angle was obtained using the front images, however, in the 3D bed the penetration angle was obtained by means of the images of the bed surface, based on the penetration ratio (Fig. 8(c)).

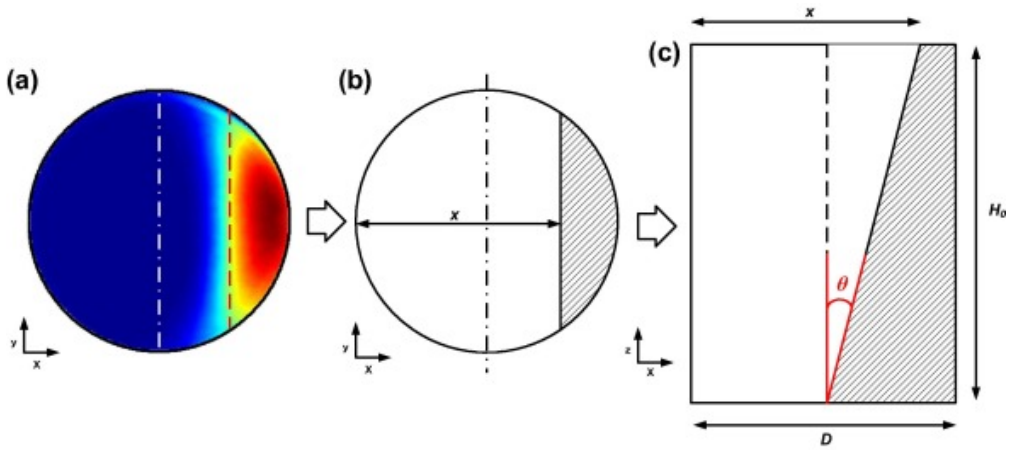

Fig. 8. Time-averaged black beads concentration on the bed surface (top view) (a), definition of the penetration ratio (b) and definition of the penetration angle (c) (3D facility).

The penetration ratio is a function of the aspect ratio and the gas velocity, as shown in Fig. 9(a). For a constant gas velocity, the variation of the penetration ratio with the aspect ratio follows a linear trend, except for the case of $H_0/D = 0.5$. Bubble coalescence is known to be enhanced by increasing the bed aspect ratio [26], [27]. As previously reported by Pallarès and Johnsson [24], the increase of the bed aspect ratio reduces the number of preferred vertical bubble paths and, consequently, the number of vortexes in the flow structure. Taking this into account, it is expected that the case with the lowest aspect ratio ($H_0/D = 0.5$) has a different bubble flow pattern, and this could be the reason why the linear trends are not followed in Fig. 9(a) provided that it is high enough to guarantee that a single preferred bubble path is generated. According to that, the $H_0/D = 0.5$ data were neglected for the following calculations.

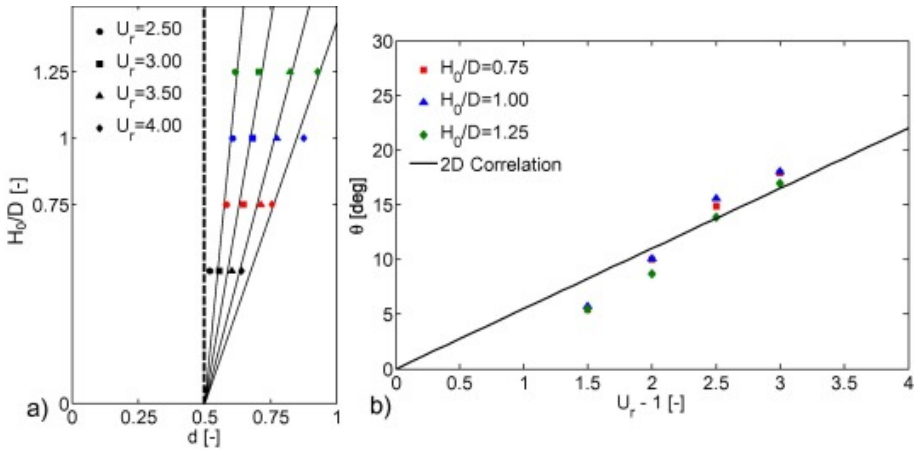

Fig. 9. Penetration ratio (a) as a function of H_0/D for different values of U_r tested and penetration angle (b) as a function of U_r for the different values of H_0/D tested (3D facility).

As for the results of the 2D facility, the penetration angle, θ, was found to be almost independent of the bed aspect ratio (Fig. 9(b)). According to that, and considering that the range of gas superficial velocities investigated in the 3D facility is similar to the range of velocities of the 2D experiments, the estimations of the correlation developed for the 2D data (Eq. (1)) were compared with the experimental data of the penetration angle measured in the 3D facility. The estimations of the correlation seem to be in good agreement with the experimental data of the 3D facility, as can be observed in Fig. 9(b) and, as a result, the correlation can be used for extrapolation purposes in the range of gas velocities investigated.

The correlation proposed can be used then to estimate the size of the defluidized zone generated by the half-covered distributor plate and to determine whether defluidization can be detected by visual inspection at the bed surface or not. For example, for a relative gas velocity of $U_r = 6.00$ the penetration angle calculated with Eq. (1) is $\theta = 27°$, which is high enough to obtain a penetration ratio of 1 with an aspect ratio of 1.25. This means that when a video of the bed surface is recorded with the aforementioned conditions, a uniform bubble concentration pattern is obtained at the bed surface; however a defluidized zone, whose size can be estimated using the calculated penetration angle, is present at the bottom zone of the fluidized bed. The penetration angle can be employed to determine the defluidized zone generated for any portion of covered distributor orifices produced during operation. The proposed correlation for the penetration angle give similar results for 2D and 3D facilities, even though the experiments were performed with different bed material and the angle was estimated using different approaches.

The defluidized volume in the 3D facility can be estimated by means of the experimental values of the penetration ratio as the resulting volume of cutting the bed with a plane with an angle equal to the corresponding penetration angle. Fig. 10 shows a schematic of the calculation of the defluidized volume. To integrate the defluidized volume, V_{def}, (blue zone in Fig. 10) the variable x_f was defined as a function of the penetration ratio (Eq. (5)).

$$x_f = (d - 0.5)D \tag{5}$$

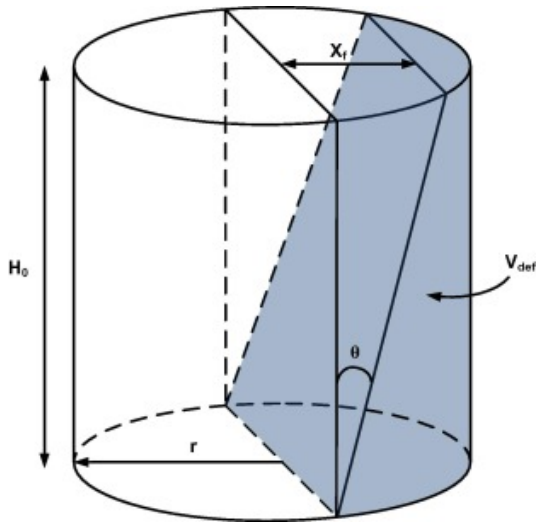

Fig. 10. Schematic of the calculation of the defluidized volume in the 3D facility.

Considering the definition of x_f, the analytical expression to determine the defluidized volume for a 3D cylindrical fluidized bed is the following:

$$V_{def} = \frac{r^2 H_0}{(x_f/r)} \left[(x_f/r)\cos^{-1}(x_f/r) - \sin(\cos^{-1}(x_f/r)) + \sin^3(\cos^{-1}(x_f/r))/3 + 2/3\right] \tag{6}$$

To evaluate the extrapolation of the 2D results to 3D beds, the experimental values of defluidized volume were compared with the estimated values obtained with correlations.

The correlation of Johnsson et al. [28] was used to estimate the visible bubble flow in a 3D bed. The results of the correlation were previously compared with measurements in a 16 MWth fluidized bed boiler at high temperature, but also with measurements in a cold 2D fluidized bed and with data found in literature for 3D beds. First, the value of f_2 is calculated with Eq. (7) as a function of the gas velocity, and then the fraction of visible bubble flow, ψ, was estimated with Eq. (8).

$$f_2 = [0.26 + 0.70\exp(-3.3d_p)][0.15 + (U_0 - U_{mf})]^{-0.33} \quad (7)$$

$$\psi = f_2(h + \sqrt{A_t/N_h})^{0.4} \quad (8)$$

where A_t is the cross sectional area of the distributor plate, in this case half of the total distributor area, and N_h is the number of distributor orifices in that section. The height over the distributor plate at which the visible bubble flow is evaluated, h, was selected to be equal to the fixed bed height, H_0. The visible bubble flow, Uvis, was calculated with Eq. (9).

$$U_{vis} = \psi(U_0 - U_{mf}) \quad (9)$$

The normalized visible bubble flow was related to the normalized defluidized volume in the previous section of this work (Fig. 7). According to that, the defluidized volume in the 3D bed was estimated with Eq. (4) using the values of visible bubble flow obtained from the correlation of Johnsson et al. [28]. The experimental values of normalized defluidized volume in the 3D bed, calculated with Eq. (6), were compared with the predicted values of the correlation proposed in this work (Eq. (4)) using the Johnsson et al. [28] correlation for the visible bubble flow. For a better comparison, the experimental and predicted results of the normalized defluidized volume were plotted together in Fig. 11.

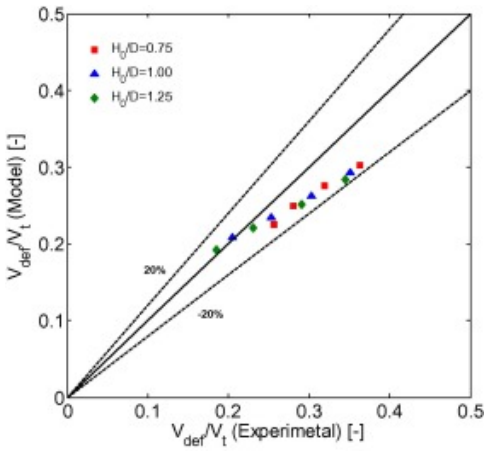

Fig. 11. Comparison between experimental and predicted values of the normalized defluidized volume in the 3D bed.

It was found that the defluidized volume in a 3D bed can be estimated with the correlations developed for 2D beds with maximum relative errors of 20%. The maximum errors were found at low relative gas velocities and the model seems to predict accurately the defluidized volume for higher bed aspect ratios and higher relative gas velocities. A trend was observed in the modeled values. Different expressions or correlations could be more suitable for this application, however the simple methodology proposed predicts the experimental results with an acceptable accuracy. The method developed in this work can be used then to estimate the size of dead zones in large-scale fluidized beds, assuming that the defluidized zone measured in the 3D facility can be seen as a dead zone produced by maldistribution and/or agglomeration. Visual inspection data of the bed surface is needed to successfully apply the model; however, as stated above, the use of IR cameras is a common practice in industry. The concentration of CO, CO_2 and H_2O is usually measured in industry. Since reactions occur in the bubble phase, a sudden increase on the concentration of gases could be related to a maldistribution problem inside the bed.

4. Conclusions

The internal structure of an induced maldistributed pseudo-2D bed was studied. The maldistribution was induced covering half of the total orifices of the distributor plate. It was found that a defluidized zone appears above the covered part of the distributor plate and a solids recirculation zone appears just above the defluidized zone. The size of the defluidized zone was obtained by means of DIA and the size of the recirculation zone was obtained by means of PIV. The experimental values of defluidized and recirculation volume were normalized with the average volume of the expanded bed. Both zones were found to be affected by the relative gas velocity and the bed aspect ratio.

The normalized defluidized volume was found to decrease with the relative gas velocity and the bed aspect ratio, while the normalized defluidized volume was found to increase with the relative gas velocity and the bed aspect ratio. The variations in the size of both zones are strongly related to the bubble phase. According to that, the visible bubble flow was obtained experimentally and a correlation was proposed to relate the normalized visible bubble flow with the normalized defluidized volume.

The penetration angle, defined as the angle between the boundary of the defluidized zone and the normal to the distributor of the bed, was determined experimentally. It was found that the penetration angle increases with the relative gas velocity following a linear trend, but seems to be independent of the bed aspect ratio. A correlation was proposed for the estimation of the penetration angle as a function of the relative gas velocity. The proposed correlation can be applied in the range of gas superficial velocities used in the experiments (U_r = 3–6).

The extrapolation of the 2D internal structure of the induced maldistributed data to a 3D bed was then investigated. Two different variables were studied: the penetration angle and the normalized defluidized volume. It was observed that, although the experiments were carried out with different bed material and the penetration angle was estimated with different methods, the correlation obtained from the 2D facility can be fairly used to fit the defluidized volume deduced from the 3D facility.

The correlation of Johnsson et al. [28] was used to calculate the normalized visible bubble flow in the 3D facility. These estimations were then used to calculate the normalized defluidized volume in a 3D bed with the proposed correlation obtained with the 2D data. The experimental values of the normalized defluidized volume in the 3D bed, calculated by integration with the experimental values of the penetration ratio and penetration angle, were compared with the estimations using correlations. It was found that the proposed methodology is capable of predicting the defluidized volume in a 3D bed with maximum relative errors of around 20%. The maximum errors were found at low relative gas velocities and the method seems to fit accurately the defluidized volume for higher aspect ratios and higher relative gas velocities. A trend was observed in the modeled values, thus other expressions or correlations should be investigated in further research.

Acknowledgements

The authors express their gratitude to the financial support from project DPI2009-10518 (MICINN – Spain). We would like to thank Professor Antonio Acosta-Iborra for his help with the integration of the defluidized volume in the 3D facility and Dr. Fernando Hernández-Jiménez for commenting on the manuscript.

Appendix A. Supplementary data

Supplementary data associated with this article can be found, in the online version, at http://dx.doi.org/10.1016/xxxxxxxxxxx.

References

[1] J.R. van Ommen, R.J. de Korte, C.M. van den Bleek, Rapid detection of defluidization using the standard deviation of pressure fluctuations, Chem. Eng. Process. 43 (2004) 1329–1335.

[2] A.B. Whitehead, D.C. Dent, Behaviour of multiple tuyere assemblies in large fluidized beds, in: A.A.H. Drinkenburg (Ed.), Proceedings of the International Symposium on Fluidisation, June 6–9; Netherlands University Press, Enindhoven, Amsterdam, 1967, p. 802.

[3] S. Fakhimi, D. Harrison, Multi-orifice distributors in fluidized beds: a guide to design, in: Chemeca ' 70, Butterworth, Australia, 1970, p. 29.

[4] P.L. Yue, J.A. Kolaczkowski, Multiorifice distributor design for fluidized beds, Trans. Inst. Chem. Eng. 60 (1982).

[5] R.B. Thorpe, J.F. Davidson, M. Pollitt, J. Smith, Maldistribution in fluidized beds, Ind. Eng. Chem. Res. 41 (2002) 5878–5889.

[6] D. Sathiyamoorthy, C.H. Sridhar Rao, The choice of distributor to bed pressure drop r atio in gas fluidised beds, Powder Technol. 30 (1981) 139–143.

[7] A.B. Whitehead, in: J.F. Davidson, D. Harrison (Eds.), Fluidization, Academic Press, London, 1971, p. 781.

[8] J. Sánchez-Prieto, A. Soria-Verdugo, J.V. Briongos, D. Santana, The effect of temperature on the distributor design in bubbling fluidized beds, Powder Technol. 261 (2014) 176–184.

[9] J. Sánchez-Prieto, A. Soria-Verdugo, J. Gómez-Hernández, J.V. Briongos, D. Santana, Maldistribution detection in bubbling fluidized beds, Chem. Eng. J.(2014).

[10] S. Zipser, A. Gommlich, J. Matthes, H.B. Keller, Combustion plant monitoring and control using infrared and video cameras, in: Power Plants and Power Systems Control, Kananaskis, Canada, 2006.

[11] M. Chimenti, C. Di Natali, G. Mariotti, E. Paganini, G. Pieri, O. Salvetti, An IR image processing approach for characterizing combustion instability, Infrared Phys. Technol. 46 (2004) 41–47.

[12] G. Lu, G. Gilabert, Y. Yan, Vision based monitoring and characterization of combustion flames, J. Phys. Conf. Ser. 15 (2005) 194–200.

[13] J. Ballester, T. García-Armingol, Diagnostic techniques for the monitoring and control of practical flames, Prog. Energy Combust. Sci. 36 (2010) 375–411.

[14] A. González-Cencerrado, B. Peña, A. Gil, Coal flame characterization by means of digital image processing in a semi-industrial scale PF swirl burner, Appl. Energy 94 (2012) 375–384.
[15] F. Hernández-Jiménez, S. Sánchez-Delgado, A. Gómez-García, A. Acosta-Iborra, Comparison between two-fluid model simulations and particle image analysis & velocimetry (PIV) results for a two-dimensional gas-solid fluidized bed, Chem. Eng. Sci. 66 (2011) 3753–3772.
[16] D. Geldart, Types of gas fluidization, Powder Technol. 7 (1973) 285–292.
[17] S.B.R. Karri, J. Werther, Gas distributor and plenum design in fluidized beds, in: C. Yang (Ed.), Handbook of Fluidization and Fluid-particle Systems, Marcel Dekker Inc., New York, 2003, pp. 164–179.
[18] J.K. Sveen, 1998–2008, MATPIV. http://www.math.uio.no/jks/matpiv/.
[19] J.A. Laverman, I. Roghair, M. van Sint Annaland, J.A.M. Kuipers, Investigation into the hydrodynamics of gas–solid fluidized beds using particle image velocimetry coupled with digital image analysis, Can. J. Chem. Eng. 86 (2008) 523–535.
[20] A. Soria-Verdugo, L.M. García-Gutiérrez, U. Ruiz-Rivas, D. Santana, Buoyancy effects on objects moving in a bubbling fluidized bed, Chem. Eng. Sci. 66 (2011) 2833–2841.
[21] T.M. Gernon, M.A. Gilbertson, R.S.J. Sparks, M. Field, Gas-fluidisation in an experimental tapered bed: insights into processes in diverging volcanic conduits, J. Volcanol. Geotherm. Res. 174 (2008) 49–56.
[22] T.M. Gernon, M.A. Gilbertson, R.S.J. Sparks, M. Field, The role of gas-fluidisation in the formation of massive volcaniclastic kimberlite, Lithos 112S (2009) 439–451.
[23] T.M. Gernon, M.A. Gilbertson, Segregation of particles in a tapered fluidized bed, Powder Technol. 231 (2012) 88–101.
[24] D. Pallarès, F. Johnsson, A novel technique for particle tracking in cold dimensional fluidized beds – simulating fuel dispersion, Chem. Eng. Sci. 61 (2006) 2710–2720.
[25] S. Sánchez-Delgado, C. Marugán-Cruz, A. Soria-Verdugo, D. Santana, Estimation and experimental validation of the circulation time in a 2D gas–solid fluidized bed, Powder Technol. 235 (2013) 669–676.
[26] R.C. Darton, R.D. LaNauze, J.F. Davidson, D. Harrison, Bubble growth due to coalescence in fluidized beds, Trans. Inst. Chem. Eng. 55 (1977) 274–288.
[27] R.J. De Korte, J.C. Schouten, C.M. Van den Bleek, Controlling bubble coalescence in a fluidized-bed model using bubble injection, AIChE J. 47 (2001) 851–860.
[28] F. Johnsson, S. Andersson, B. Leckner, Expansion of a freely bubbling fluidized bed, Powder Technol. 68 (1991) 117–123.